Soft Matter

Accepted Manuscript

This is an *Accepted Manuscript*, which has been through the Royal Society of Chemistry peer review process and has been accepted for publication.

Accepted Manuscripts are published online shortly after acceptance, before technical editing, formatting and proof reading. Using this free service, authors can make their results available to the community, in citable form, before we publish the edited article. We will replace this *Accepted Manuscript* with the edited and formatted *Advance Article* as soon as it is available.

You can find more information about *Accepted Manuscripts* in the **Information for Authors**.

Please note that technical editing may introduce minor changes to the text and/or graphics, which may alter content. The journal's standard **Terms & Conditions** and the **Ethical guidelines** still apply. In no event shall the Royal Society of Chemistry be held responsible for any errors or omissions in this *Accepted Manuscript* or any consequences arising from the use of any information it contains.

Anisotropic Colloidal Transport and Periodic Stick-Slip Motion in Cholesteric Finger Textures

Kui Chen, Linnea P. Metcalf, David P. Rivas, Daniel H. Reich, and Robert L. Leheny

Department of Physics & Astronomy, Johns Hopkins University, Baltimore, Maryland, 21218

ABSTRACT

We have investigated the mobility of discoidal colloidal particles sedimenting within cholesteric finger textures formed by mixtures of the nematic liquid crystal 4-cyano-4'-pentylbiphenyl (5CB) and the chiral dopant 4-(2-methylbutyl)-4'-cyanobiphenyl (CB15) with cholesteric pitch p between 24 and 114 μm. The nickel disks, with radius 17 μm and thickness 300 nm, displayed varied transport behavior that depended on the size of the pitch and the orientation of the gravitational force with respect to the cholesteric axis. In textures with small pitch ($p < 40$ μm), the disks moved perpendicular to the axis irrespective of the orientation of gravity as a result of an elastic retarding force that prevented motion along the axis. In textures with larger pitch, the disks similarly moved perpendicular to the axis when the angle between the force and axis was large. When the angle was small, the disks displayed stick-slip motion caused by periodic yielding of the finger texture. A model considering viscous drag on the particles and the elastic energy cost of deforming the finger texture describes the stick-slip motion accurately. The effective drag viscosities obtained from the disk motion are anomalously large compared with those of pure nematic 5CB indicating a large contribution to the dissipation from the motion of disclinations in the texture in the vicinity of the translating disks.

1

I. Introduction.

Understanding the mobility of colloidal particles in structured fluids is a major goal of soft matter physics. Typically, the drag forces and other interactions that a particle experiences in a structured fluid are significantly subtler and more complicated than the Stokes drag from a simple Newtonian fluid.[1-3] The resulting dynamics can provide insightful, microscopic perspectives into the properties of the fluid. They can also form the foundation for new technologies in areas such as self-assembly, separations, and sensing. For example, nematic liquid crystals are fluids with a broken symmetry caused by alignment of the fluid molecules along a common direction specified by the director $n(r)$. As a consequence of this symmetry breaking, the mobility of a colloid becomes dependent on its direction of motion through the fluid such that the effective drag viscosity is different when the colloid moves parallel versus perpendicular to $n(r)$.[4-17] The magnitude of the drag is further sensitive to the nature of the distortion that the colloid imposes on the local director field, which in turn depends on the anchoring conditions for the director at the particle surface dictated by surface chemistry.[5, 6, 18] A striking consequence of this drag anisotropy is the creation of a dynamic "nematic lift" force, in which a colloid moving through a nematic at an oblique angle to the director acquires a velocity component perpendicular to the applied force.[5, 8] The sensitivity of this lift force to the anchoring suggests a novel route for separating particles according to surface chemistry.

In addition to the nematic phase, liquid crystals can form other broken symmetry states whose ordering should have further consequences for the mobility of colloids. For example, in a cholesteric liquid crystal the director assumes a helical twist with a pitch p that breaks translational symmetry. Distortions in this order imposed by a suspended particle lead to interparticle interactions and colloidal assemblies not seen in nematics,[19-33] in part because the distortion to the order depends not only on the anchoring conditions at the particle surface but also on the size of the particle relative to the pitch.[25, 34] Further, recent studies have shown how the size dependence affects dynamics, specifically by making the drag force on a sphere moving through a cholesteric a nonlinear function of the sphere radius in contrast with Stokes Law.[25, 35] Here we report an experimental investigation of the mobility of discoidal colloidal particles in frustrated cholesterics known as finger textures that are characterized by a periodic array of disclinations in the order. Exploring motion in the frustrated cholesteric enables us to investigate

both colloidal mobility in a fluid with broken translational symmetry and the effect of interactions between defects in the order and the colloids on the colloid dynamics. The choice of disks, rather than for example spheres, was made because the discoidal shape enabled us to investigate particle sizes that were relatively large, at least in two dimensions, with respect to the cholesteric pitch in textures with large domains of uniform order. We find the particle mobility to be highly anisotropic, with the presence of a weak "yield force" that resists motion along one direction in the fluid. The strength of this yield force depends on the size of the pitch relative to the particle. When the driving force exceeds the yield force, the particles experience stick-slip motion that can be understood as a consequence of a periodic elastic retardation imposed by the fluid.

II. Experimental Procedures

The mobility of the disk-shaped colloidal particles in the finger textures was characterized by classic "falling ball" experiments in which the drag on a particle with a density larger than that of the surrounding fluid is measured by balancing it with gravity, as illustrated in Fig. 1. Cholesteric liquid crystals with micrometer-scale pitch were created by mixing nematic 4-cyano-4'-pentylbiphenyl (5CB) with the chiral dopant 4-(2-methylbutyl)-4-cyanobiphenyl (CB15). The cholesteric pitch p was adjusted by varying the weight concentration c of CB15 following the formula $p = \frac{1}{f \cdot c}$, where f =7.3 μm^{-1} is the macroscopic helical twisting power. Mixtures with pitches between 24 and 114 μm were included in the study. A dilute suspension of colloidal nickel disks was added to the cholesteric by first incorporating the disks into the 5CB. The disks, with radius R = 17 μm and thickness d = 300 nm, had homeotropic surface anchoring introduced through functionalization with dimethyloctadecyl[3-(trimethoxysilyl)propyl]ammonium chloride (DMOAP). Methods for fabricating the disks and their behavior in nematic 5CB have been reported previously.[36]

To create the finger textures, the cholesteric containing the disks was loaded into sample cells comprised of parallel glass substrates treated with indium tin oxide (ITO) to make them conductive and with DMOAP to achieve homeotropic anchoring. Plastic spacers set the cell thickness. The thickness was chosen for each sample to be approximately equal to the

cholesteric pitch since matching these length scales helps in creating well-ordered textures. The chiral structure of the cholesteric is frustrated by the homeotropic anchoring condition at the substrates. As a result, the director field assumes a distorted configuration that nevertheless preserves the periodicity of the cholesteric. Four different metastable textures, known as finger textures, have been identified for cholesterics in homeotropic cells.[37, 38] The prevalence of each depends on parameters such as the strength of the anchoring, the elastic constants of the liquid crystal, and the strength of any external electric field. The texture that has the lowest energy under most conditions and hence is the most commonly observed is known as CF-1,[38] and the conditions in our experiment led to the formation of this texture. In the CF-1 texture, the cholesteric axis orients parallel to the substrates, and each period contains two pairs of closely positioned non-singular $\lambda^{+1/2}$ and $\lambda^{-1/2}$ disclinations that run perpendicular to the cholesteric axis, as depicted schematically in Fig. 1.[38] To obtain uniformly aligned textures with periodic arrays of straight disclinations over a large area, we applied electric and magnetic fields to the sample in tandem following established procedures.[39] An AC electric field with amplitude 4.2×10^5 V/m and frequency 1 kHz was applied across the ITO-treated substrates for 5 minutes in the presence of a magnetic field of approximately 1 T parallel to the substrates at room temperature. After the electric field was removed, the cell was kept in the magnetic field for an additional sixty minutes. An example of the resulting well-aligned cholesteric finger texture is shown in Fig. 2.

To conduct the experiments, we tilted an optical microscope (Nikon TS100) by 90º so that the force of gravity $\boldsymbol{F_g}$ on the disks was parallel to the microscope's focal plane, as shown schematically in Fig. 1. The magnitude of this force was

$$F_g = \pi R^2 d(\rho_{Ni} - \rho_{5CB})g = 21 \text{ pN} \qquad (1)$$

where $\rho_{Ni} = 8,900$ kg/m^3 is the density of nickel, $\rho_{5CB} = 1,020$ kg/m^3 is the density of 5CB, and g is the gravitational constant. The liquid crystal cells were mounted on the microscope with their substrates parallel to the focal plane and could be rotated about the optical axis to vary the angle α between the cholesteric axis and gravity, thereby enabling determination of the colloid mobility along various directions with respect to the cholesteric axis. The disks were imaged as they translated through the microscope's field of view using a 10x/0.25 objective and a single-lens reflex camera (Nikon D3100). When suspended in the cholesteric, the disks assumed

positions near the center of the cells and oriented such that the faces of the disks were parallel to the substrates, presumably due to elastic interactions with the substrates.[36, 40-42]

III. Results

The mobility of the disks in the cholesteric finger textures showed a strong dependence on the size of the pitch. At small pitch ($p < 40 \mu$m), the disk motion was exclusively perpendicular to the cholesteric axis regardless of the orientation of the applied force, and a force parallel to the axis resulted in no motion. Thus, the elastic forces associated with distortions of the texture balanced the component of gravity along the cholesteric axis. However, in textures with larger pitch, the dynamics were complex as the gravitational force was sufficient to overcome the elastic retardation along the axis, leading in some cases to stick-slip motion. In the sections below, we describe the nature of the motion for various conditions of pitch size and direction of applied force that illustrate this highly anisotropic and pitch-dependent mobility, and we present a model that describes the stick-slip dynamics.

A. Sedimentation Force Perpendicular to Cholesteric Axis

The simplest behavior was observed when the gravitational force was oriented perpendicular to the cholesteric axis and hence parallel to the disclinations ($\alpha = \pi/2$). In this case, the disks moved at a constant velocity v parallel to the force. Figure 2 displays a series of bright-field micrographs showing a disk moving in this direction in a texture with $p = 62$ μm. (The video from which these micrographs were obtained is available as part of the Supplementary Information as S1_alpha90.avi.) Since the motion was at low Reynolds number (Re ~ 10^{-6}), this constant velocity implied that drag forces from viscous dissipation $\boldsymbol{F_d}$ balanced gravity, $\boldsymbol{F_d} = -\boldsymbol{F_g}$. For a disk translating in a simple isotropic liquid, the drag force would be given by Stokes law,

$$\boldsymbol{F_d} = -\zeta \boldsymbol{v} = -\frac{32}{3} R \eta \boldsymbol{v}, \qquad (2)$$

where $\zeta = \frac{32}{3} R \eta$ is the drag coefficient for a disk[43], and η is the liquid's shear viscosity. From the velocity of the sedimenting disk in the cholesteric, one can employ Eq. (2) to obtain an

effective drag viscosity η_{eff} that characterizes the dissipation. We stress that the application of Eq. (2), with $\zeta = \frac{32}{3} R \eta_{eff}$ to describe the drag on the disk in the cholesteric, is not strictly valid. Due to the broken orientational and translational symmetry of the cholesteric, the flow field around the disk and hence the nature of the drag are more complicated than those of an isotropic liquid for which Stokes law is derived. In particular, as discussed further below, the disk mobility depends strongly on the relative size of R and p, indicating a distinctly non-Stokesian character to the motion. Nevertheless, we employ the Stokes form to describe the drag since it provides a measure of the drag in a familiar form that allows easy comparisons of the dissipation experienced under different circumstances. For example, for the motion depicted in Fig. 2, we obtain η_{eff} = 420 mPa·s. Similar values were found for disks moving perpendicular to the cholesteric axis in textures with different p. This effective drag viscosity is strikingly large compared with that describing colloidal motion in nematic 5CB where, depending on the direction of motion with respect to the nematic director and the anchoring conditions at the particle surface, drag viscosities vary between 25 mPa·s and 110 mPa·s, which fall in the range of the Miesowicz coefficients of 5CB.[5, 8] We attribute the anomalously large drag in the finger textures to dissipation associated with motion of the disclinations lines, which must deform in the vicinity of the disk as it falls, as illustrated in Fig. 2.

To test this idea, we conducted similar sedimentation measurements on silica spheres and nickel nanowires in finger textures. The spheres deformed the texture considerably as they translated perpendicular to the cholesteric axis and experienced anomalously large drag. For instance, silica spheres with approximate radius of 5 μm and planar surface anchoring in a 40-μm-pitch texture experienced an effective drag viscosity of 720 mPa·s. In contrast, the wires, which had longitudinal surface anchoring[41] and oriented with their axis perpendicular to the cholesteric axis, created no observable distortion of the texture and sedimented with an effective drag viscosity that was similar to the values in pure 5CB.[5] Specifically, the effective drag viscosity experienced by a 10-μm-long Ni wire with diameter 350 nm translating in 70-μm-pitch texture was approximately 150 mPa·s.

B. Sedimentation Force Parallel to Cholesteric Axis

When the force of gravity was oriented parallel to the cholesteric axis ($\alpha = 0$), the viscous response of the texture was accompanied by spatially varying elastic contributions whose strength depended on the cholesteric pitch. In textures with small pitch ($p < 40$ μm), the disks remained stationary ($v = 0$). We interpret this lack of motion as due to a balance between the elastic forces associated with distortion of the texture and gravity. In textures with larger pitch, the elastic forces, while still present, were insufficient to balance gravity and instead the disks underwent periodic stick-slip motion.   Figure 3, which displays a series of bright-field micrographs of a disk in a texture with 60-μm pitch, illustrates this motion. (The video from which these micrographs were obtained is available as part of the Supplementary Information as S2_alpha0.avi.) A set of disclination lines in each micrograph is highlighted in red. As the disk passed through the disclinations, they temporarily attached to the disk. As a result, the disk distorted the texture, stretching the disclinations as it fell. Eventually, the disk detached from the disclinations, allowing the texture to recover from the distortion.   As the disk stretched the disclinations, its motion was increasingly retarded.   Then, when it detached, it briefly moved relatively unencumbered until it encountered the next set of disclinations, and the process repeated. Figure 4(a) displays the height and velocity as a function of time of a disk undergoing this motion as it traversed three periods of the texture with $p = 60$ μm. During each period, the velocity steadily decreased, corresponding to when the disk stretched the disclinations, and then suddenly jumped to a larger value, signaling detachment. In Sec. IV below, we present a model that describes this periodic stick-slip motion.

C. Sedimentation Force at Oblique Angle to Cholesteric Axis

When the gravitational force was oriented at an oblique angle to the cholesteric axis, the resulting disk motion contained elements of the behavior seen in both the perpendicular and parallel configurations, and the nature of the motion depended both on the pitch size and on the angle α between the force and the axis. In textures with large p at small α, the motion was similar to that when the force was parallel to the axis: the disks translated parallel to the driving force with periodic stick-slip motion. However, at large α the component of gravity parallel to the cholesteric axis was sufficiently small that the elastic forces associated with distorting the texture could balance it. The resulting motion in this case is illustrated in Fig. 5, which displays

a series of micrographs of a disk in a texture with p = 60 µm and α = 70º. (The video from which these micrographs were obtained is available as part of the Supplementary Information as S3_alpha70.avi.) Instead of undergoing stick-slip motion, the disk remained near one set of disclinations and moved parallel to the disclinations (and hence at an angle α to the applied force) at constant velocity. Assuming that the force causing this motion was the component of gravity perpendicular to the cholesteric axis (parallel to the disclinations), we can again interpret the constant velocity as the result of a balance between the driving force and drag forces from viscous dissipation, $\boldsymbol{F_d}$ = - $\boldsymbol{F_g}\sin(\alpha)$. Further, to quantify this dissipation we can again adapt Stokes law, Eq. (2), to obtain an effective drag viscosity. From the velocity of the disk in the texture with p = 60 µm and α = 70º shown in Fig. 5, we obtain a very large value, η_{eff} = 1080 mPa·s. (We again stress that this quantity should not be considered literally as the shear viscosity of the cholesteric but rather as a measure of the dissipation for comparison with other sedimentation conditions.) As before, we interpret this large dissipation as the consequence of contributions from motion of the disclination lines, which experience considerable deformation by the moving disk at this orientation of the texture.

The range of angles α at which the disks either displayed stick-slip motion or moved at a constant velocity parallel to the disclinations depended on the size of the pitch. For small pitch, where no stick-slip motion was observed even at α = 0, the disk velocity was parallel to the disclinations at all α (except at α = 0 where the component of gravity parallel to the disclinations was zero and hence the velocity was zero). For larger pitch and at intermediate α, the disk dynamics could be considered a hybrid of the two types of motion seen at large and small α. That is, during their motion the disks moved parallel to the disclinations and hence at an angle to the applied force at times, but the texture also periodically yielded so that the disks could traverse the texture from one period to the next. Figure 6, which displays a series of bright-field micrographs of a disk in a texture with p = 114 µm at α = 42º, illustrates this motion. (The video from which these micrographs were obtained is available as part of the Supplementary Information as S4_alpha42.avi.) Figure 7(a) shows the zigzag trajectory made by the disk depicted in Fig. 6, while Fig. 7(b), which shows its time-dependent velocity as it traversed two periods of the texture, illustrates its stick-slip motion. Notably, the disk's direction of motion as it traversed each period of the texture unencumbered by the disclinations was not strictly vertical

and parallel to gravity but instead was oriented farther toward the cholesteric axis. We attribute this deflection of the velocity from the direction of the applied force to a lift force created by the anisotropic drag in these regions of the texture.

IV. Model for Stick-Slip Motion

As the descriptions above illustrate, the response of the cholesteric finger texture to colloidal motion is highly anisotropic and non-Stokesian. A key ingredient of this response is the behavior of the periodic array of disclinations, whose distortion gives rise to the anomalously large drag and to the stick-slip motion. To model the forces that create the stick-slip motion, we characterized the distortions in the texture by measuring the length and positions of the sets of disclinations in the vicinity of sedimenting disks undergoing the motion. From these measurements we identified two contributions to the elastic energy cost of distorting the texture: one from stretching the disclinations and one from compressing the cholesteric pitch. However, as described in the Appendix, in modeling the effect of these energy costs on the disk motion, we found that the contribution from the compression could be neglected. For simplicity, we therefore focus on the stretching energy, which we approximate as

$$U_s = T \sum_i \Delta L_i = T \Delta L_{total} \; , \tag{3}$$

where ΔL_i is the excess length of the ith set of disclinations, and T is the energy per unit length, or line tension, of the disclinations. For example, Fig. 4(b) depicts the time-dependent length ΔL in excess of the undistorted length of the five sets of disclinations labeled in Fig. 3(a) along with their sum ΔL_{total}. This energy cost leads to a force on a disk,

$$F_e = -\frac{dU_s}{dy} = -T \frac{d(\Delta L_{total})}{dy}, \tag{4}$$

where y is the vertical position of the disk. Figure 8 displays the results for ΔL_{total} from Fig 4(b) plotted as a function of y. We note that the oscillating nature of ΔL_{total} implies that the direction of F_e similarly oscillates. In contrast, one might expect that this force, which is associated with stretching the disclinations, acts on a disk only when it is actually stretching the disclinations and ΔL_{total} is increasing, and that the elastic energy stored in the disclinations is lost to viscous dissipation as they retract. However, measurements of the stick-slip motion in textures with

large p, where the motion of the disks when they were not touching any disclinations could be clearly resolved, showed that during this part of the motion the disks actually accelerated, suggesting the presence of an increasing downward force working in conjunction with gravity. The oscillating nature of ΔL_{total} captures both the retarding nature of the disk's interaction with the disclinations due to stretching and this downward force.

In addition, we model the viscous dissipation during the stick-slip motion by a Stokes drag, Eq. (2). At low Reynolds number, the gravitational force on the disk is hence balanced by these elastic and drag forces, leading to an equation of motion for the disk,

$$F_g = F_d + F_e = \frac{32}{3}R\eta_{eff}v + T\frac{d(\Delta L_{total})}{dy} \tag{5}$$

In principle, one can solve this equation to obtain a prediction for the position of the disk as a function of time. However, because of the scatter in ΔL_{total}, direct differentiation of the data to obtain F_e is impractical. Therefore, to compare the model with the data, we integrate Eq. (5) to obtain:

$$y_2 - y_1 = \frac{32R}{3F_g}\eta_{eff}\int_{y_1}^{y_2} vdy + \frac{T}{F_g}[\Delta L_{total}(y_2) - \Delta L_{total}(y_1)], \tag{6}$$

where y_1 and y_2 are two values of the disk's position. Using the values of the disk velocity from Fig. 4(a) and the excess length of the disclinations from Fig. 8 as inputs, we fit Eq. (6) to the data for the disk position with η_{eff} and T as free parameters. The result of the fit, shown by the solid red line in Fig. 4(a), agrees closely with the measurements.

The best fit value for the effective viscosity, η_{eff} = 600 mPa·s, again indicates an anomalously large drag reflecting the dissipation associated with motion of the disclinations. The best fit value for the disclination line tension, T = 13.6 pN, can be compared with the theoretically expected [44] tension of the four (nonsingular) λ-disclinations in each period of the finger texture:

$$T = 4\pi K s^2 \ln\left(\frac{L}{r_c}\right) \tag{7}$$

where $K \approx 5$ pN is the average Frank elastic constant of 5CB,[45] $s = 1/2$ is the strength of the λ disclinations, L is the effective size of the system, and r_c is the disclination core radius. The core

radius of the λ-disclinations is approximately the pitch p.[46] Taking L to be the spacing between the substrates, we hence expect $\ln\left(\frac{L}{r_c}\right)$ to be of order one, and hence the tension to be a few times K, which is in good agreement with the fit result. Further, from T and estimates of $\frac{d(\Delta L_{total})}{dy}$ at the yield points, we find that the maximum stretching force at yielding is approximately 12 ± 2 pN for $p = 60$ μm. This yield force, which depends on the pitch, derives from several factors including K and the strength of the anchoring at the particle surface. Its important feature is its similarity to the sedimentation force F_g, which leads to the complex dynamics displayed by the disks.

As the remarkable agreement between the model for the stick-slip motion (Eq. (6)) and the measured results for the disk position demonstrates, the model appears to capture the key ingredients involved in causing the periodic motion through the finger texture. This agreement is perhaps surprising given the simplicity of the model and the approximations that it makes. For example, by approximating the viscous dissipation in terms of a single effective viscosity through Stokes Law, the model neglects the full complexity of viscous drag in liquid crystals. As mentioned in the Introduction, the drag on a colloidal particle moving in a liquid crystal depends on its direction of motion with respect to the surrounding director field. Since the orientation of the director varies as a function of position within each period of the finger texture, the viscous drag on the disk should similarly vary with position. This spatial variation is compounded by the contribution to the dissipation from the motion of the disclinations, which also varies as the disk traverses each period in the stick-slip motion. In addition, due to the spatial variation of the director field in the cholesteric texture, the distortion imposed on the director by the disk beyond stretching the disclinations should vary with position, and hence the elastic energy cost of that distortion should also vary. Such a gradient in distortion energy should further give rise to a force on the particles.[41, 42, 47] As mentioned above, the form of F_e includes both a retarding force when the disks are attached the disclinations and stretching them as well as an accelerating force during detachment, and this accelerating component could be serving to approximate some of these effects. Nevertheless, the good agreement between the model prediction and the data in Fig. 4(a) demonstrates that the overwhelming contribution to the forces on the disk in the finger texture that creates the stick-slip motion is from interactions with the disclinations.

V. Conclusion

In conclusion, these experiments to investigate the mobility of discoidal particles in cholesteric finger textures have illustrated the novel behavior that can occur as part of sedimentation within structured fluids. The broken translational symmetry of the finger textures and the organized array of defects that are inherent to the textures provide a means to spatially modulate mobility in a way that is sensitive to the size of the particles relative to the structural length scales that characterize the fluid. Further, the ability of the disclinations in the texture to redirect the disks away from the direction of externally applied forces (such as gravity) illustrates the potential of such particle-defect interactions for manipulating colloids. In particular, while the ability to channel colloidal particles through their interactions with defects, for example in microfluidic environments, has been demonstrated previously,[48] the present work highlights the varied behavior that can occur when these interactions compete with other forces. Experiments that explore the possibility of similar phenomena in colloidal transport within other structured fluids with broken translational symmetry and ordered defects, such as the blue phase of liquid crystals and smectic liquid crystals in wedge samples, would test the generality of this behavior and its potential for applications.

Appendix: Compression Energy

A noteworthy feature of the disk's effect on the texture was that not only did the disclinations attached to the disk change length as the disk fell but so did nearby disclinations. For instance, during the time the set of disclinations labeled C in Fig. 3 were in contact with the disk (the time interval 420 s < t < 800 s in Fig. 4(b)), not only did ΔL of that set of disclinations go through a maximum as the disk stretched them and then detached but so did ΔL for the set of disclinations immediately below the disk, labeled D, and to a lesser extent the next set below,

labeled E. We associate the distortion of these neighboring disclinations with the tendency of the finger texture to maintain a preferred periodicity. This preference implies an energy cost to compressing (or expanding) the texture, which we approximated as

$$U_{compress} = B \sum_i \int (h_i(s) - p)^2 \, ds, \tag{8}$$

where the integral is along the contour of each set of disclinations, $h_i(s)$ is the perpendicular distance from the local contour of set i of disclinations to the next set, $i+1$, and B is a coefficient setting the compression energy. As mentioned above, in modeling the effect of the energy costs associated with distorting the texture on the disk motion, we found that the contribution from this compression energy could in fact be neglected. That is, the quality of fits using the model to describe the data was statistically indistinguishable when we set $B = 0$ and when we allowed B to be a free parameter.
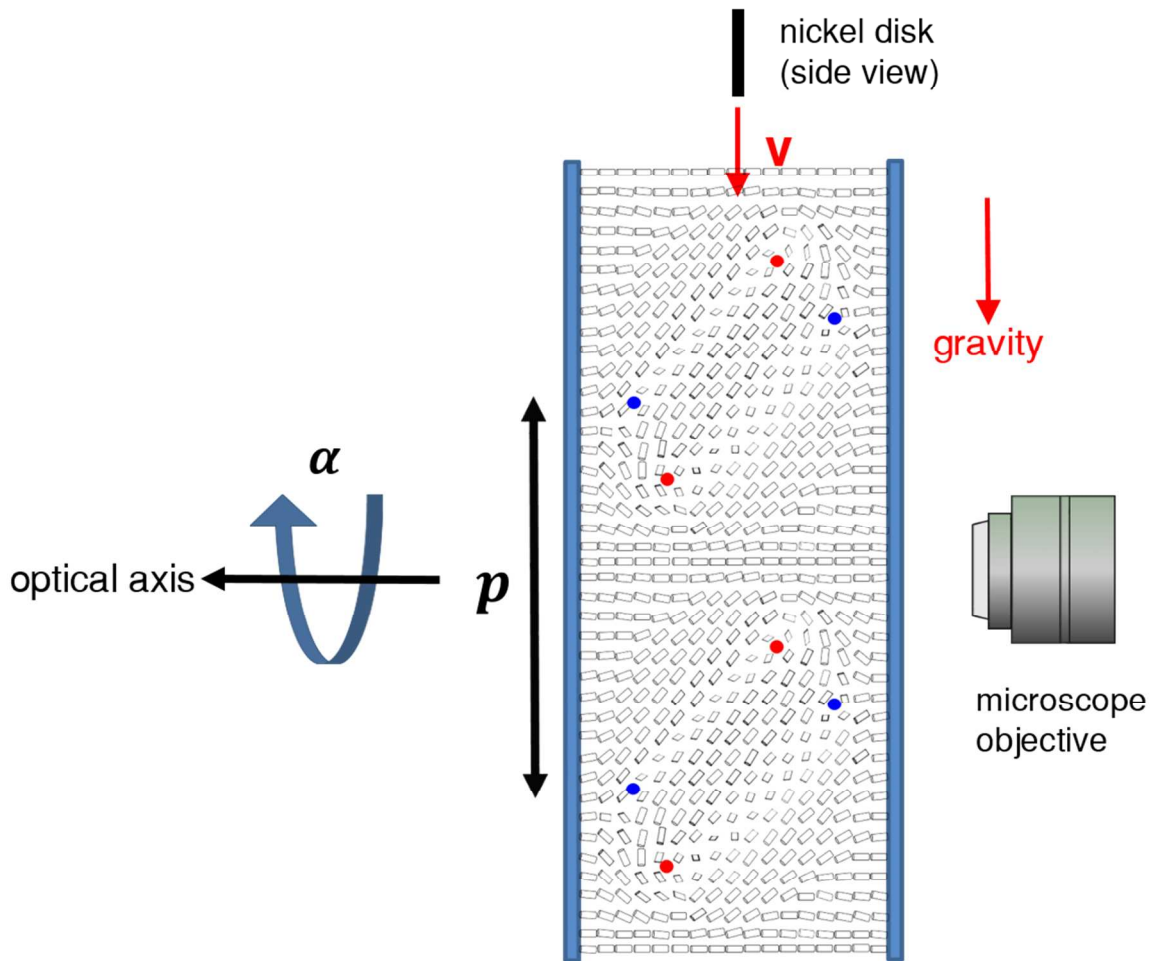
Figure 1. Schematic of the sedimentation experiments. The microscope was tilted 90º to make the driving force (gravity) parallel to the focal plane. Strong homeotropic anchoring at the surfaces of the glass slides (blue) caused the cholesteric liquid crystal with pitch p to assume a distorted CF-1 finger texture. The local director orientation within the texture, which is depicted by the cylinders, includes nonsingular $\lambda^{+1/2}$ (red dots) and $\lambda^{-1/2}$ (blue dots) disclinations. (Schematic of finger texture adapted from Reference 38.)
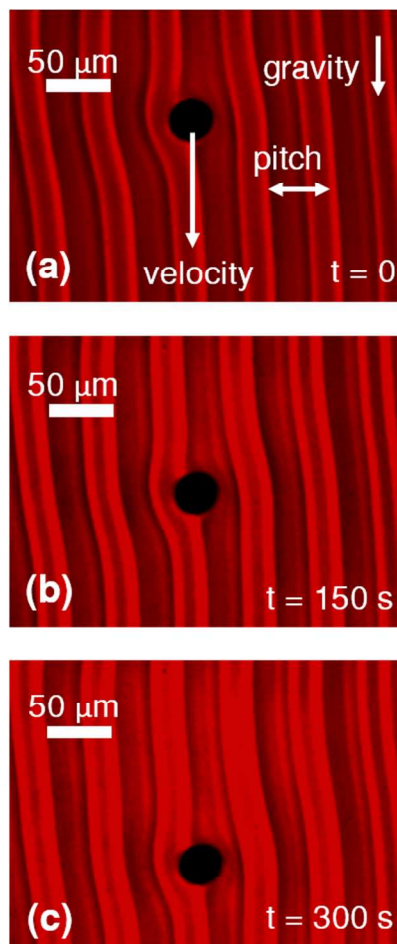
Figure 2. Images of a Ni disk sedimenting through a cholesteric finger texture with a 62-μm pitch. The disk velocity is parallel to gravity, which is perpendicular to the cholesteric axis. The texture distorts in the vicinity of the moving disk, increasing the drag. The time interval between successive images is 150 s.
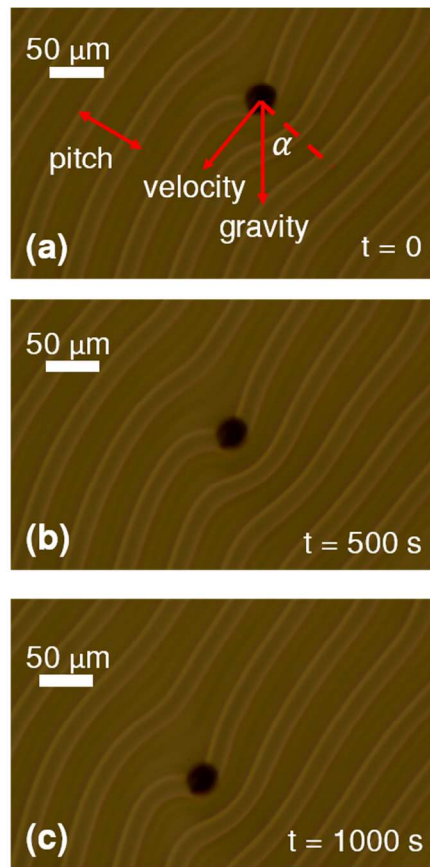
15
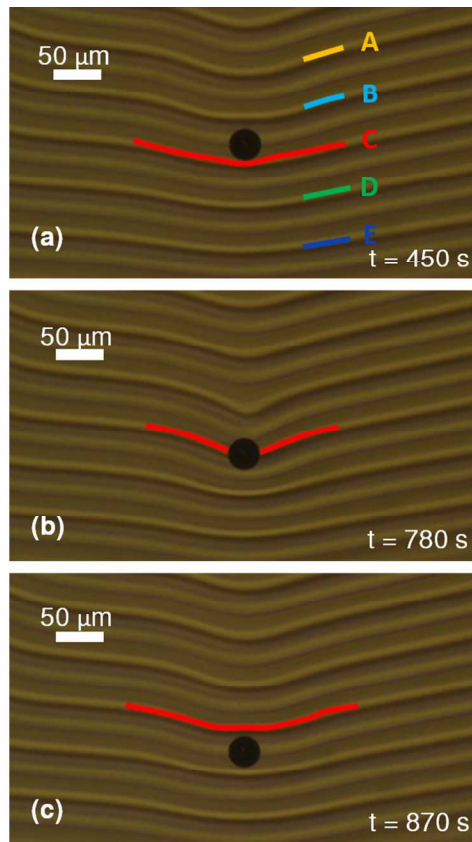
Figure 3. Images of a Ni disk sedimenting through a cholesteric finger texture with 60-µm pitch in response to gravity parallel to the cholesteric axis. Five sets of disclination lines are labeled A through E in (a). The contour of one set, labeled C, is depicted in red in all three images to illustrate the time-dependent distortion of the texture as the disk undergoes stick-slip motion. The time in each image matches the time axis of Fig. 4.
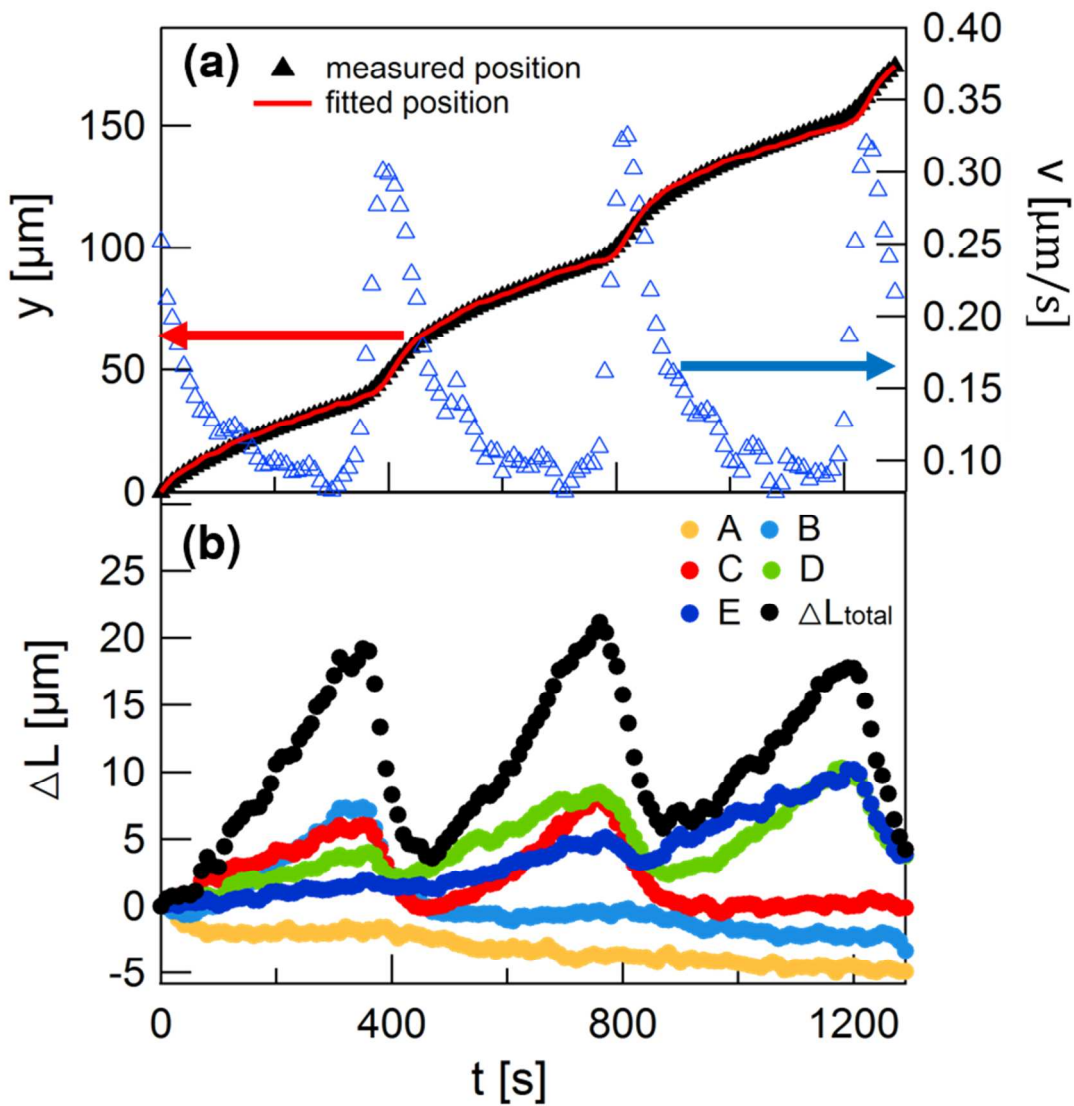
Figure 4. (a) Position (solid triangles) and velocity (open triangles) of the disk shown in Fig. 3 sedimenting through a 60-μm-pitch figure texture in response to gravity parallel to the cholesteric axis. Downward in the images in Fig. 3 is taken as the positive y direction. The solid red line is the result of a fit to the position using the model described in Sec. IV. (b) The lengths of the disclination lines labeled in Fig. 3(a) in excess of their undistorted lengths along with the sum of the excess lengths.

Figure 5. Images of a Ni disk sedimenting through a cholesteric finger texture with 60-μm pitch in response to gravity oriented at an angle $\alpha = 70°$ to the cholesteric axis. The disk moves perpendicular to the axis. The time interval between successive images is 500 s.
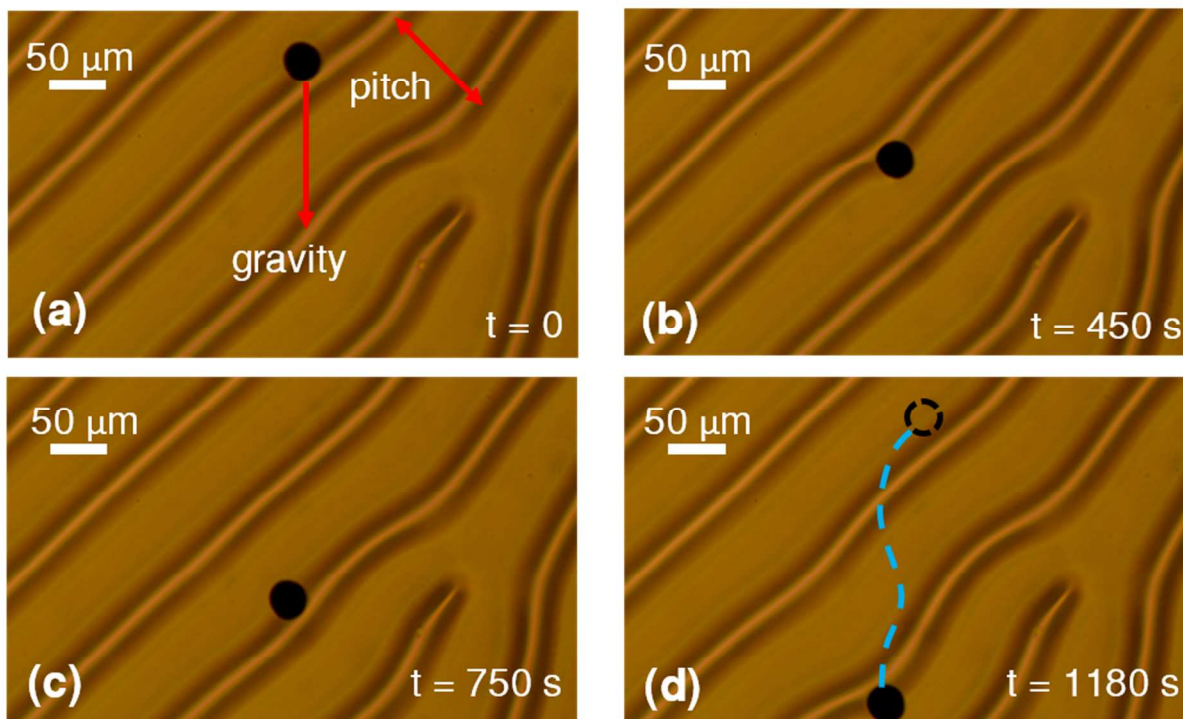
Figure 6. Images of a Ni disk sedimenting through a cholesteric finger texture with 114-µm pitch in response to gravity oriented at an angle $\alpha = 42°$ to the cholesteric axis. The time in each image matches the time axis of Fig. 7(b). The dashed line in (d) denote the trajectory of the disk.
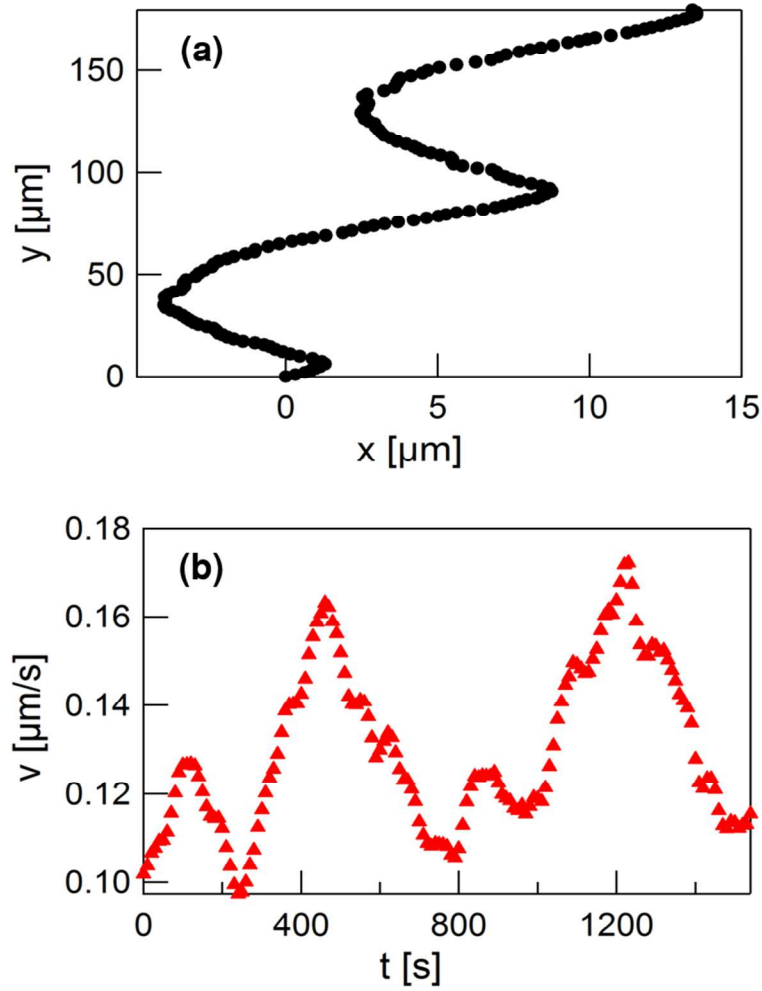
Figure 7. (a) Trajectory and (b) magnitude of velocity of the nickel disk in Fig. 6 sedimenting through a cholesteric finger texture with 114-µm pitch in response to gravity oriented at an angle $\alpha = 42°$ to the cholesteric axis. Note the positive-y direction is defined as downward (parallel to gravity).

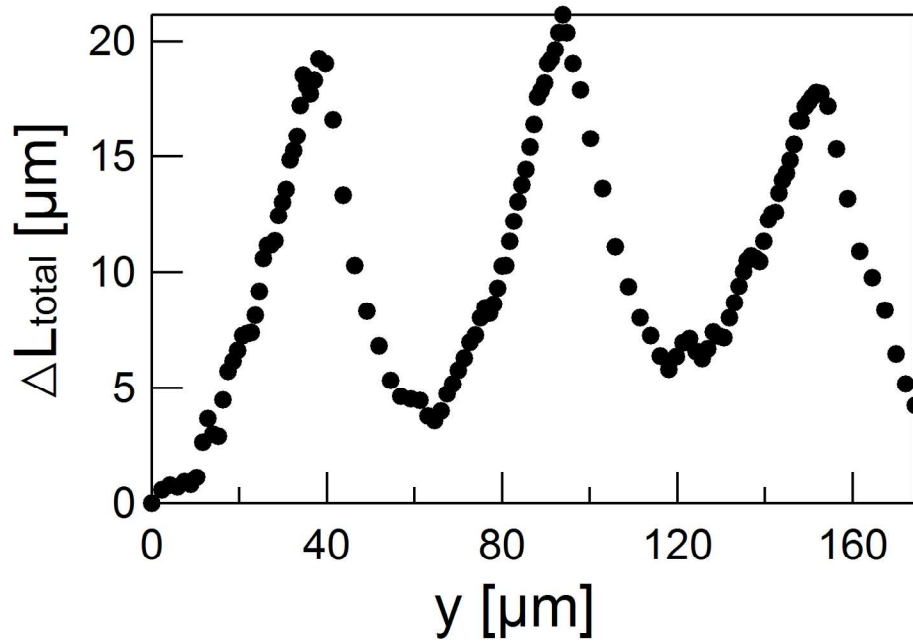**Figure 8.** Total excess length of the disclinations ΔL_{total} from Fig. 4(b) plotted as a function of disk height.

References:

1. H. Stark and D. Ventzki, *Europhys. Lett.*, 2002, **57**, 60-66.
2. O. D. Lavrentovich, *Soft Matter*, 2014, **10**, 1264-1283.
3. T. Turiv, I. Lazo, A. Brodin, B. I. Lev, V. Reiffenrath, V. G. Nazarenko and O. D. Lavrentovich, *Science*, 2013, **342**, 1351-1354.
4. J. C. Loudet, P. Hanusse and P. Poulin, *Science*, 2004, **306**, 1525-1525.
5. J. B. Rovner, C. P. Lapointe, D. H. Reich and R. L. Leheny, *Phys. Rev. Lett.*, 2010, **105**, 228301.
6. R. W. Ruhwandl and E. M. Terentjev, *Phys. Rev. E*, 1996, **54**, 5204-5210.
7. H. Stark and D. Ventzki, *Phys. Rev. E*, 2001, **64**, 031711.
8. J. B. Rovner, D. H. Reich and R. L. Leheny, *Langmuir*, 2013, **29**, 2104-2107.
9. T. Araki and H. Tanaka, *J. Phys.: Condens. Matter*, 2006, **18**, L193-L203.
10. J. A. Moreno-Razo, E. J. Sambriski, G. M. Koenig, E. Diaz-Herrera, N. L. Abbott and J. J. de Pablo, *Soft Matter*, 2011, **7**, 6828-6835.
11. D. Abras, G. Pranami and N. L. Abbott, *Soft Matter*, 2012, **8**, 2026-2035.
12. H. F. Gleeson, T. A. Wood and M. Dickinson, *Philos. Trans. R. Soc. London, Ser. A*, 2006, **364**, 2789-2805.
13. F. Mondiot, J. C. Loudet, O. Mondain-Monval, P. Snabre, A. Vilquin and A. Wurger, *Phys. Rev. E*, 2012, **86**, 010401.
14. R. W. Ruhwandl and E. M. Terentjev, *Z. Naturforsch. A*, 1995, **50**, 1023-1030.
15. M. Skarabot and I. Musevic, *Soft Matter*, 2010, **6**, 5476-5481.
16. A. A. Verhoeff, J. van Rijssel, V. W. A. de Villeneuve and H. N. W. Lekkerkerker, *Soft Matter*, 2008, **4**, 1602-1604.
17. B. Senyuk, D. Glugla and I. I. Smalyukh, *Phys. Rev. E*, 2013, **88**, 062507.
18. G. M. Koenig, R. Ong, A. D. Cortes, J. A. Moreno-Razo, J. J. de Pablo and N. L. Abbott, *Nano Lett.*, 2009, **9**, 2794-2801.
19. N. Hijnen, T. A. Wood, D. Wilson and P. S. Clegg, *Langmuir*, 2010, **26**, 13502-13510.
20. F. E. Mackay and C. Denniston, *EPL*, 2011, **94**, 66003.
21. M. Ravnik, G. P. Alexander, J. M. Yeomans and S. Zumer, *Faraday Discuss.*, 2010, **144**, 159-169.
22. J. C. Loudet, P. Barois, P. Auroy, P. Keller, H. Richard and P. Poulin, *Langmuir*, 2004, **20**, 11336-11347.
23. U. Tkalec, M. Ravnik, S. Zumer and I. Musevic, *Phys. Rev. Lett.*, 2009, **103**, 127801.
24. M. Mitov, C. Portet, C. Bourgerette, E. Snoeck and M. Verelst, *Nature Mater.*, 2002, **1**, 229-231.
25. J. S. Lintuvuori, K. Stratford, M. E. Cates and D. Marenduzzo, *Phys. Rev. Lett.*, 2010, **105**, 178302.
26. M. Ravnik, G. P. Alexander, J. M. Yeomans and S. Zumer, *Proc. Natl. Acad. Sci.*, 2011, **108**, 5188-5192.
27. M. B. Pandey, P. J. Ackerman, A. Burkart, T. Porenta, S. Žumer and I. I. Smalyukh, *Phys. Rev. E*, 2015, **91**, 012501.
28. J. S. Lintuvuori, K. Stratford, M. E. Cates and D. Marenduzzo, *Phys. Rev. Lett.*, 2011, **107**, 267802.
29. S. Copar, T. Porenta, V. S. R. Jampani, I. Musevic and S. Zumer, *Soft Matter*, 2012, **8**, 8595-8600.

30.	J. S. Lintuvuori, A. C. Pawsey, K. Stratford, M. E. Cates, P. S. Clegg and D. Marenduzzo, *Phys. Rev. Lett.*, 2013, **110**, 187801.
31.	A. C. Pawsey, J. S. Lintuvuori, T. A. Wood, J. H. J. Thijssen, D. Marenduzzo and P. S. Clegg, *Soft Matter*, 2012, **8**, 8422-8428.
32.	F. E. Mackay and C. Denniston, *Soft Matter*, 2014, **10**, 4430-4435.
33.	K. Stratford, O. Henrich, J. S. Lintuvuori, M. E. Cates and D. Marenduzzo, *Nat Commun*, 2014, **5**, 3954.
34.	M. Melle, S. Schlotthauer, C. K. Hall, E. Diaz-Herrera and M. Schoen, *Soft Matter*, 2014, **10**, 5489-5502.
35.	M. C. M. Varney, Q. Zhang, M. Tasinkevych, N. M. Silvestre, K. A. Bertness and I. I. Smalyukh, *Phys. Rev. E*, 2014, **90**, 062502.
36.	J. B. Rovner, D. S. Borgnia, D. H. Reich and R. L. Leheny, *Phys. Rev. E*, 2012, **86**, 041702.
37.	J. Baudry, S. Pirkl and P. Oswald, *Phys. Rev. E*, 1998, **57**, 3038-3049.
38.	I. Smalyukh, B. Senyuk, P. Palffy-Muhoray, O. Lavrentovich, H. Huang, E. Gartland, V. Bodnar, T. Kosa and B. Taheri, *Phys. Rev. E*, 2005, **72**, 061707.
39.	T. Ishikawa and O. Lavrentovich, *Phys. Rev. E*, 1999, **60**, R5037-R5039.
40.	C. Lapointe, N. Cappallo, D. H. Reich and R. L. Leheny, *J. Appl. Phys.*, 2005, **97**, 10Q304.
41.	C. Lapointe, A. Hultgren, D. M. Silevitch, E. J. Felton, D. H. Reich and R. L. Leheny, *Science*, 2004, **303**, 652-655.
42.	O. P. Pishnyak, S. Tang, J. R. Kelly, S. V. Shiyanovskii and O. D. Lavrentovich, *Phys. Rev. Lett.*, 2007, **99**, 127802.
43.	F. M. White, *Fluid Mechanics*, WCB McGraw Hill, Boston, 4th edn., 1999.
44.	P. G. de Gennes and J. Prost, *The Physics of Liquid Crystals*, Clarendon Press, Oxford, 1993.
45.	N. V. Madhusudana and R. Pratibha, *Mol. Cryst. Liq. Cryst.*, 1982, **89**, 249-257.
46.	M. Kleman and O. D. Lavrentovich, *Soft Matter Physics: An Introduction (Partially Ordered Systems)*, Springer, New York, 2003.
47.	C. P. Lapointe, D. H. Reich and R. L. Leheny, *Langmuir*, 2008, **24**, 11175-11181.
48.	A. Sengupta, C. Bahr and S. Herminghaus, *Soft Matter*, 2013, **9**, 7251-7260.
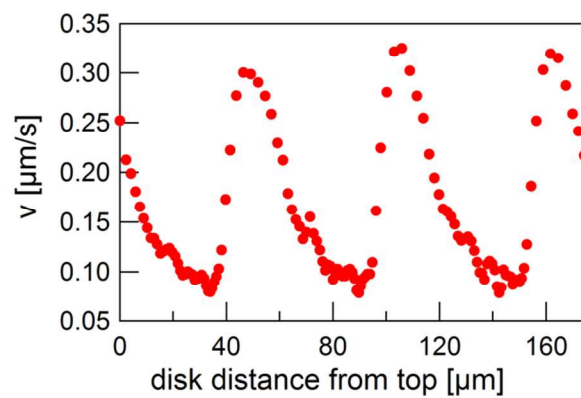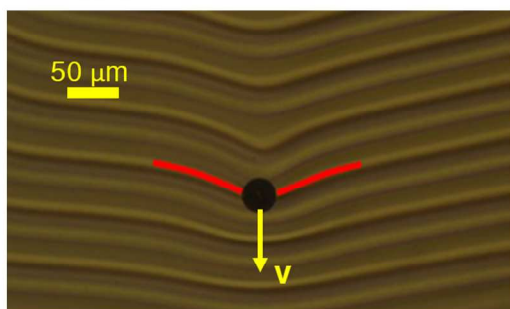
TOC Figure: Particles sedimenting in cholesteric finger textures display an array of behavior including non-Stokesian dynamics and stick-slip motion.